

## Dependence of neutron yield on fragment mass for several low-energy fissioning systems

J. Gindler

Chemistry Division, Argonne National Laboratory, Argonne, Illinois 60439

(Received 23 October 1978)

Neutron-yield functions for  $^{245}\text{Cm}(n,f)$ ,  $^{252}\text{Cf}(sf)$ ,  $^{254}\text{Cf}(sf)$ ,  $^{254}\text{Es}(n,f)$ , and  $^{256}\text{Fm}(sf)$  are derived with an iterative method in which successive approximations to the pre-neutron-emission (initial) mass distribution are compared with the post-neutron-emission (final) mass distribution. Initial mass distributions are deduced from kinetic energy measurements of the fragments. Final mass distributions are determined from radiochemical measurements of fission product mass yields. The  $^{252}\text{Cf}(sf)$  neutron-yield function so derived agrees well with functions determined directly by neutron counting. All neutron-yield functions exhibit a saw-toothed character. The masses for which maximum neutron emission occurs and for which minimum neutron emission occurs are within  $\pm 2$  mass units of being complementary masses for the observed fissioning system, with the exception of the  $^{245}\text{Cm}(n,f)$  reaction. The effect of the neutron-yield function on various mass and energy correlations deduced from kinetic energy measurements is discussed.

[NUCLEAR REACTIONS, FISSION  $^{245}\text{Cm}(n,f)$ ,  $^{252}\text{Cf}(sf)$ ,  $^{254}\text{Cf}(sf)$ ,  $^{254}\text{Es}(n,f)$ ,  $^{256}\text{Fm}(sf)$ . Deduced neutron yields, fragment mass and energy distributions.]

### I. INTRODUCTION

The dependence of neutron yield on the mass of the fission fragment,  $\bar{\nu}(M)$ , has been determined directly from neutron-counting experiments for a number of fissioning systems. For low-energy fission, that is, spontaneous fission (sf) or thermal-neutron-induced fission ( $n,f$ ), a saw-toothed dependence has been demonstrated for  $^{252}\text{Cf}(sf)$ ,<sup>1-8</sup>  $^{233}\text{U}(n,f)$ ,<sup>9,10</sup>  $^{235}\text{U}(n,f)$ ,<sup>9-15</sup> and  $^{239}\text{Pu}(n,f)$ .<sup>9,13</sup> This saw-toothed dependence has also been deduced indirectly from simultaneous measurements of the velocities and kinetic energies of the fission fragments,<sup>16-21</sup> from differences in the yields of pre- and post-neutron-emission fragment mass distributions,<sup>22-24</sup> and from post-neutron-emission fragment mass distributions alone.<sup>22,25</sup>

The general similarity among neutron-yield functions for the four low-energy fissioning systems led Terrell<sup>22</sup> to suggest that a universal neutron-yield function exists for which the number of neutrons emitted approaches zero at closed-shell nuclei of fifty neutrons or protons and which also may be affected by the eighty-two neutron shell. The idea of a universal  $\bar{\nu}(M)$  was questioned by Apalin *et al.*<sup>11</sup> since the maximum neutron yield occurs at fragment masses 110 for  $^{235}\text{U}(n,f)$  and 120-122 for  $^{252}\text{Cf}(sf)$ . This apparent difference, however, may arise because of the small yields associated with masses in the region of near-symmetrical fission in  $^{235}\text{U}(n,f)$  with the result that few, if any, neutrons are detected for masses in this region. Therefore, to determine whether a universal neutron-yield function does exist or whether the neutron-yield function varies from one fissioning system to another,  $\bar{\nu}(M)$  has been

determined for four other fissioning systems:  $^{245}\text{Cm}(n,f)$ ,  $^{254}\text{Cf}(sf)$ ,  $^{254}\text{Es}(n,f)$ , and  $^{256}\text{Fm}(sf)$ .

In these systems, symmetric or near-symmetric fission is considerably more probable than in the systems studied heretofore. This affords a better examination of any systematic trends in the character of  $\bar{\nu}(M)$  in this mass region. Furthermore, one may examine the effect of  $\bar{\nu}(M)$  on mass distributions deduced for fissioning systems of the heavy actinides. These distributions have generally been deduced from kinetic energy (KE) measurements of coincident fragments with either no correction made for neutron emission from the fragments (provisional mass distributions) or with the assumption that  $\bar{\nu}(M)$  for a given system is shaped like that for  $^{252}\text{Cf}(sf)$ . The present paper examines in detail the effect of  $\bar{\nu}(M)$  on the mass distribution and various energy distributions as well.

The neutron-yield functions have been determined from differences in mass yields deduced from KE measurements and from radiochemical (RC) measurements of the fission products. The advantage of this method is that it permits the determination of  $\bar{\nu}(M)$  for systems in which the target or fissioning nuclide is available in less than microgram amounts. The validity of the method was checked by deriving  $\bar{\nu}(M)$  for  $^{252}\text{Cf}(sf)$  and comparing this function with those determined by direct neutron counting. The KE and RC measurements used in this work were made primarily at Argonne National Laboratory. Therefore, any systematic errors made in collecting the data should affect the determination of  $\bar{\nu}(M)$  for each system in a similar manner. As a result, the different neutron-yield functions should be relatively if not absolutely correct.

## II. METHOD

The method used to calculate  $\bar{\nu}(M)$  is essentially that of Terrell's<sup>22</sup> in which initial (pre-neutron-emission) and final (post-neutron-emission) cumulative yields of fission fragments are matched. The cumulative yield in this sense means the sum of the yields of all fragments with mass up through a given value. For mass  $M_0$  the initial and final cumulative yields are defined as  $\sum_0^{M_0} y(M)$  and  $\sum_0^{M_0} Y(M)$ , respectively.

The relationship between the initial and final fragment yields derived by Terrell is

$$\sum_0^{M_0 - \bar{\nu}(M_0) - 1/2} Y(M) = \sum_0^{M_0 - 1/2} y(M) + \frac{1}{2} (dy/dM) \langle \sigma^2(\bar{\nu}(M); M) \rangle + \dots, \quad (1)$$

in which both  $\bar{\nu}(M)$  and the slope  $(dy/dM)$  are evaluated at  $M_0$ . Conditional variances  $\langle \sigma^2(\bar{\nu}(M); M) \rangle$  have been determined by Terrell<sup>22</sup> for the four fissioning systems,  $^{233}\text{U}(n, f)$ ,  $^{235}\text{U}(n, f)$ ,  $^{239}\text{Pu}(n, f)$ , and  $^{252}\text{Cf}(sf)$ . In the present paper the variances for the fissioning systems studied have been deduced by a linear interpolation or extrapolation of Terrell's variances plotted as a function of the average number of neutrons emitted per fission ( $\bar{\nu}_T$ ) for the fissioning system. Values of  $\bar{\nu}_T$  and the variances used in this work are listed in Table I. Although the correction term  $\frac{1}{2}(dy/dM)\langle \sigma^2(\bar{\nu}(M); M) \rangle$  has been included in Eq. (1) it usually has a

TABLE I. Parameters used in the calculation of  $\bar{\nu}(M)$  for the fissioning systems.

System	$\bar{\nu}_T^a$	$\langle \sigma^2(\bar{\nu}(M); M) \rangle^b$
$^{233}\text{U}(n, f)$	2.49 <sup>c</sup>	$0.56 \pm 0.3^d$
$^{235}\text{U}(n, f)$	2.42 <sup>c</sup>	$0.61 \pm 0.3^d$
$^{239}\text{Pu}(n, f)$	2.88 <sup>c</sup>	$0.66 \pm 0.3^d$
$^{252}\text{Cf}(sf)$	3.77 <sup>c</sup>	$0.76 \pm 0.4^d$
$^{245}\text{Cm}(n, f)$	3.832 <sup>e</sup>	0.77 <sup>f</sup>
$^{254}\text{Cf}(sf)$	3.89 <sup>g</sup>	0.77 <sup>f</sup>
$^{254}\text{Es}(n, f)$	4.26 <sup>h</sup>	0.83 <sup>f</sup>
$^{256}\text{Fm}(sf)$	3.73 <sup>i</sup>	0.76 <sup>f</sup>

<sup>a</sup>Average number of neutrons emitted per fission.

<sup>b</sup>Average variance of the neutron yield for a given fragment mass.

<sup>c</sup>Recommended value from Hanna *et al.*, Ref. 26, rounded to the nearest hundredth.

<sup>d</sup>Value determined by Terrell, Ref. 22.

<sup>e</sup>Value from Jaffey and Lerner, Ref. 27.

<sup>f</sup>Value deduced by extrapolation or interpolation. See text.

<sup>g</sup>Average value from Manero and Konshin, Ref. 28.

<sup>h</sup>Value deduced from systematics of Jaffey and Lerner, Ref. 27.

<sup>i</sup>Value from Dakovskii *et al.*, Ref. 29.

small effect<sup>22</sup> in the determination of  $\bar{\nu}(M)$ . Therefore, higher-order terms have been neglected. To obtain  $\bar{\nu}(M)$  for all values of initial mass  $M$ , it is necessary to match the cumulative initial fragment yields corrected by the term given in Eq. (1) to the cumulative final yields. This is done by interpolating smoothly between discrete values of the cumulative final mass distribution.<sup>22</sup>

Since the initial mass distributions are derived from KE measurements of complementary fragments and these measurements are made after neutron emission occurs, one needs to know the neutron-yield function of the fissioning system to correct the kinetic energies of the final fragments into kinetic energies of the initial fragments. However, the neutron-yield functions of the fissioning systems under investigation are not known. To resolve this paradox it was initially assumed that the neutron-yield function was shaped (in most cases) like the  $^{252}\text{Cf}(sf)$  neutron-yield function determined by Bowman *et al.*<sup>2</sup> but normalized to give the value of  $\bar{\nu}_T$  shown in Table I for the appropriate fissioning system. This neutron-yield function was designated NU(0) and permitted the calculation of a "starting" initial mass distribution YI(0) from the KE measurements described in Ref. 30. Recorded event-by-event pulse heights of the complementary fragments were converted into the kinetic energies of final fragments by means of a mass-dependent energy calibration based on a  $^{252}\text{Cf}(sf)$  fragment spectrum.<sup>31</sup> The kinetic energies of the final fragments were transformed into kinetic energies of the initial fragments by correcting for the average effects of neutron emission from the fragments using the assumed neutron-yield function and including the dependence of  $\bar{\nu}(M)$  on the total kinetic energy release. Initial fragment masses were then calculated from the initial kinetic energies by applying the conservation laws for mass and linear momentum. The resulting mass distribution was corrected<sup>32,33</sup> for mass dispersion effects associated with (1) the angular distribution of emitted neutrons on fragment recoil velocities, (2) the energy resolution of the fragment detectors, and (3) the energy loss in the target material.

The "starting" initial mass distributions deduced in the manner just described are shown as the dashed curves in Figs. 1(a)–1(e). Since the correction for dispersive effects tends to accentuate statistical fluctuations in the uncorrected mass distribution, the latter was first smoothed for the  $^{254}\text{Es}(n, f)$  and  $^{256}\text{Fm}(sf)$  systems before the correction was applied. For these two systems only 50 000 and 10 000 coincident fission events were collected, respectively. For each of the other fissioning systems more than  $10^5$  events

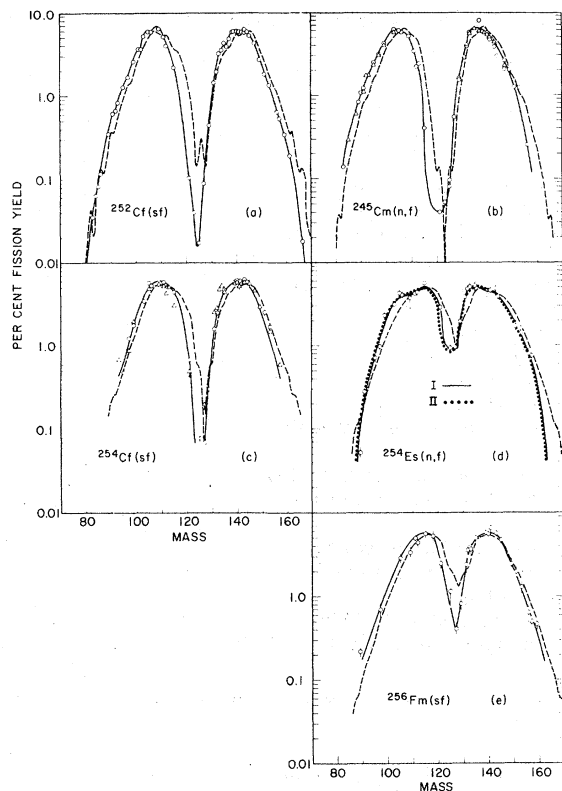


FIG. 1. Starting initial (dashed curves) and final (solid curves) mass distributions for the fissioning systems (a)  $^{252}\text{Cf}(sf)$ , (b)  $^{245}\text{Cm}(n,f)$ , (c)  $^{254}\text{Cf}(sf)$ , (d)  $^{254}\text{Es}(n,f)$ , and (e)  $^{256}\text{Fm}(sf)$ . The structure shown in the dashed curves for yields less than 1.0% are the result of statistical fluctuations in kinetic energy measurements of the fragments. In (d) the solid curve represents the final mass distribution,  $^{254}\text{Es}(n,f)$ -I, and the dotted curve represents the final mass distribution,  $^{254}\text{Es}(n,f)$ -II. The open symbols represent the mass-yield data of various investigative groups as described in the text.

were analyzed, and the correction for mass dispersion was applied directly to the uncorrected mass distribution without prior smoothing.

Final mass distributions used in the present work are shown as solid curves in Figs. 1(a)–1(e). These distributions were deduced from fission yields determined radiochemically or by mass or  $\gamma$ -ray spectrometry. All of these methods are referred to as RC measurements in the present paper. The RC measurements determine the mass of the final product unambiguously, but the method does have limitations. Generally yields with uncertainties from 5 to 15% are determined for fewer than 30 masses out of approximately 80. The Terrell method requires in an asymmetric mass distribution that the yield of the light- or heavy-mass group sums to 100% or that the total yield of both groups sums to 200%. It is therefore ob-

vious that a rather large number of yields must be determined by interpolation and that these interpolations must be made between yields that probably have sizable errors. In such a procedure it is possible to miss any fine structure that may exist in the final mass distribution.

In Figs. 1(a)–1(e) the measured fission yields are shown as open symbols. The solid curves represent mass distributions that sum to 200% total yield. For  $^{252}\text{Cf}(sf)$  the recommended yields of Flynn, Gindler, and Glendenin<sup>34</sup> are shown. These yields represent the combined measurements of their own and four other groups.<sup>35–38</sup> For  $^{245}\text{Cm}(n,f)$  the yield measurements of von Gunten, Flynn, and Glendenin<sup>39</sup> are shown as circles and those of Harbour and MacMurdo<sup>40</sup> as triangles. Since both groups employed the  $R$  method in which ratios of measured activities and unknown yields for a given fission product in the  $^{245}\text{Cm}(n,f)$  reaction were compared with measured activities and known yields for the same fission product in the  $^{235}\text{U}(n,f)$  reaction, the  $^{245}\text{Cm}(n,f)$  yields were recalculated using values of the  $^{235}\text{U}(n,f)$  yields reported by Walker.<sup>41</sup> The close agreement between the two sets of yields after the calculation just described is evidenced in Fig. 1(b). The yields shown in Fig. 1(c) for  $^{254}\text{Cf}(sf)$  were obtained at this laboratory<sup>42</sup> (circles) and at Los Alamos<sup>43</sup> (triangles). The data depicted in Fig. 1(d) for  $^{254}\text{Es}(n,f)$  are those of Flynn, Gindler, Glendenin, and Sjöblom.<sup>44</sup> In this figure the solid curve represents the one given in Ref. 44. The dotted curve represents an alternative mass distribution consistent with the data. It also sums to 200% total yield. These two distributions (solid curve and dotted curve) are referred to hereafter as distributions I and II, respectively. The data for  $^{256}\text{Fm}(sf)$  shown in Fig. 1(e) are those of Flynn *et al.*<sup>45</sup> The yield of mass 125 was re-evaluated for those fissioning systems in which the yield of this mass was determined originally by measuring the activity of the 9.6-day  $^{125}\text{Sn}$  isomer. A ratio of isomer yield to total chain yield of  $0.476 \pm 0.067$ , based on the measured ratio in  $^{252}\text{Cf}(sf)$ ,<sup>34</sup> was assumed in the re-evaluation.

The procedure for determining the neutron-yield function  $\bar{\nu}(M)$  as well as the “ending” (or last derived as opposed to starting) initial mass distribution was to deduce a first approximation for  $\bar{\nu}(M)$  by the Terrell method from the starting initial mass distribution and the final mass distribution shown in Figs. 1(a)–1(e) for a given fissioning system. Let this first approximation to  $\bar{\nu}(M)$  be called NU(1). (The nomenclature used in describing the various neutron-yield functions and mass distributions is given in Table II.) Using NU(1) a new initial mass distribution was calculated

TABLE II. Nomenclature to describe various neutron and mass functions in the iterative procedure.

Function designation	Description
NU( <i>i</i> )	Neutron-yield function. Index <i>i</i> = 0 represents the starting function, generally a function with the same shape as the <sup>252</sup> Cf(sf) neutron-yield function determined in Ref. 2. Index <i>i</i> = <i>n</i> represents the ending or last-derived function. For <i>i</i> > 0, NU( <i>i</i> ) is derived from YI( <i>i</i> -1) and the final RC mass distribution.
YI( <i>i</i> )	Initial or pre-neutron-emission mass distribution. Index <i>i</i> represents the distribution derived with KE measurements of the fission fragments and NU( <i>i</i> ).
YF( <i>i</i> )	Final or post-neutron-emission mass distribution. Index <i>i</i> represents the distribution derived with YI( <i>i</i> ) and NU( <i>i</i> ).
a or b	These subindices are used with the index <i>i</i> for the <sup>252</sup> Cf(sf) system. Index a indicates that the starting neutron-yield function, NU(0) was the function determined in Ref. 2. Index b indicates that NU(0) was a constant equal to $\bar{\nu}_T/2$ .

from the KE measurements. Let this new initial mass distribution be called YI(1). To determine the appropriateness of both NU(1) and YI(1), YI(1) was transformed into a final mass distribution YF(1) by means of a computer program that allowed the average number of neutrons determined for NU(1) to be emitted from each fragment mass determined for YI(1). The neutrons were assumed to be emitted with a normal distribution about the average  $\bar{\nu}(M_0)$  value. The variance of the neutron distribution for each fragment mass was assumed to be the same as the one given in Table I for each fissioning system. The transformed, final mass distribution YF(1) was then compared with the final mass distribution deduced from RC measurements [solid curves in Figs. 1(a)–1(e)]. If the comparison was satisfactory, then NU(1) and YI(1) were assumed to be representative for that particular fissioning system. If the comparison was not satisfactory, then another neutron-yield function NU(2) was calculated by the Terrell method using YI(1) and the final mass distribution deduced from RC measurements. The second approximation to the initial mass distribution YI(2) was then calculated from the KE measurements and NU(2), and then transformed into final mass distribution YF(2). The comparison between YF(2) and the RC final mass distribution again was made. In this iterative manner the neutron-yield function and initial mass distribution corresponding, respectively, to NU(*n*)

and YI(*n*) were determined.

For the present paper the comparison between the transformed, final mass distribution YF(*i*), where *i* may have a value from 0 through *n*, and the one deduced from RC measurements was a subjective one in which good agreement was obtained for both the light- and heavy-mass peaks and reasonably good agreement was obtained in the far-asymmetric and near-symmetric regions of the mass distributions. The most sensitive criterion as to whether particular NU(*i*) and YI(*i*) were accepted or rejected was the agreement between YF(*i*) and the RC final mass distribution in the near-symmetric mass region.

### III. RESULTS AND DISCUSSION

#### A. <sup>252</sup>Cf(sf) neutron-yield function

Since  $\bar{\nu}(M)$  has been determined for <sup>252</sup>Cf(sf) by direct neutron counting,<sup>1-8</sup> it was decided to check the procedure described in the previous section by deriving  $\bar{\nu}(M)$  for this fissioning system. Also, since the starting initial mass distribution YI(0) was calculated from the KE measurements and the neutron-yield function NU(0) determined by Bowman *et al.*<sup>2</sup> for <sup>252</sup>Cf(sf), it was to be expected that the transformed, final mass distribution YF(0) would correspond closely with the one determined from RC measurements. Therefore, to check the uniqueness of the derived neutron-yield functions, two different starting NU(0) func-

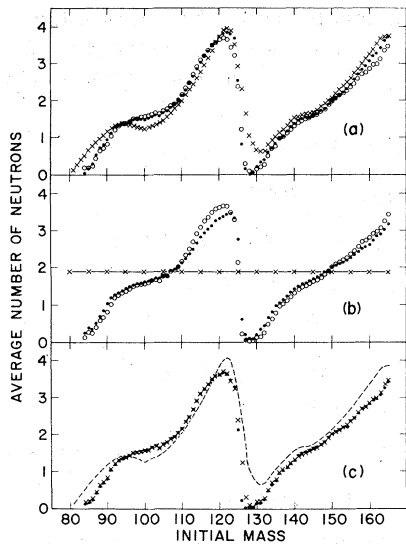


FIG. 2. Neutron-yield functions determined for  $^{252}\text{Cf}(\text{sf})$ . (a) Functions derived with the iterative method. Crosses represent the starting function,  $\text{NU}(0a)$ , which is the function determined by Bowman *et al.* (Ref. 2); solid circles, the first-derived function,  $\text{NU}(1a)$ ; open circles, the last-derived or ending function,  $\text{NU}(na)$ . (b) Functions derived with the iterative method. Crosses represent the starting function,  $\text{NU}(0b)$ ; solid circles,  $\text{NU}(1b)$ ; open circles,  $\text{NU}(nb)$ . (c) Comparison of neutron yield functions. Crosses represent  $\text{NU}(na)$ ; solid circles,  $\text{NU}(nb)$ ; dashed curve, the function determined in Ref. 2.

tions were used to initiate the iterative calculations:  $\text{NU}(0a)$ , the neutron-yield function determined experimentally by Bowman *et al.*<sup>2</sup>; and  $\text{NU}(0b)$ , a constant value equal to  $\bar{\nu}_T/2$  or 1.885. These two functions are shown as crosses in Figs. 2(a) and 2(b), respectively. The solid circles in these figures represent the first-derived neutron-yield functions,  $\text{NU}(1a)$  and  $\text{NU}(1b)$ . It is noteworthy that the  $\text{NU}(1b)$  function exhibits a strong saw-toothed dependence on mass even though  $\text{NU}(0b)$  was constant. The open circles in Figs. 2(a) and 2(b) represent the last-derived or ending neutron-yield functions,  $\text{NU}(na)$  and  $\text{NU}(nb)$ . The transformed, final mass distributions,  $\text{YF}(0a)$  and  $\text{YF}(0b)$ , are shown as crosses in Figs. 3(a) and 3(b), respectively. The solid curves in these figures represent the mass distribution determined from RC measurements. One notes in Fig. 3(a) that the transformed, final yield  $\text{YF}(0a)$  calculated with the neutron-yield function determined by Bowman *et al.*<sup>2</sup> agrees well with the RC mass distribution. The circles in Figs. 3(a) and 3(b) represent the transformed, final mass distributions,  $\text{YF}(na)$  and  $\text{YF}(nb)$ . The transformed data fit the RC mass distributions very well. It would appear that the transformed data could be made to fit the RC mass distribution exactly by suitable

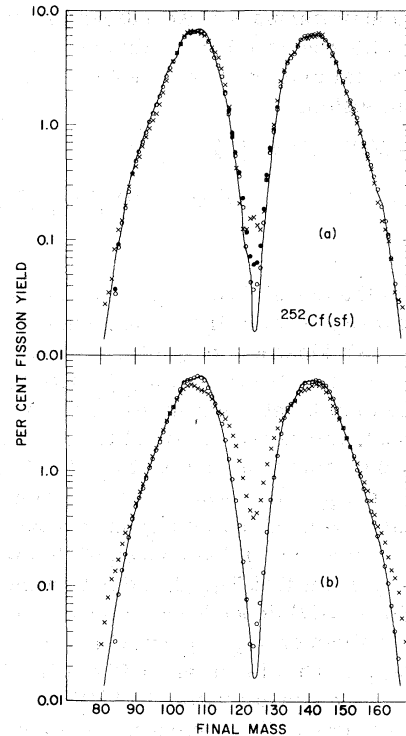


FIG. 3. Final mass distributions for  $^{252}\text{Cf}(\text{sf})$ . The solid curves in both (a) and (b) represent the RC mass distribution shown in Fig. 1(a). The crosses represent starting transformed, final mass distributions,  $\text{YF}(0a)$  and  $\text{YF}(0b)$ . The open circles represent ending transformed final mass distributions,  $\text{YF}(na)$  and  $\text{YF}(nb)$ . The solid circles in (a) represent the final mass distribution obtained from the transformation of  $\text{YI}(na)$  calculated with Eqs. (2)–(5) as explained in the text.

manipulation of the neutron-yield function. However, because of the sizable errors associated with the RC measurements, statistically fewer KE events in the low yield regions, and uncertainties associated with the variances used to correct for mass dispersion and neutron emission, further calculations to achieve an exact fit are hardly justified.

In Fig. 2(c) the two derived neutron-yield functions,  $\text{NU}(na)$  and  $\text{NU}(nb)$ , and the one determined experimentally by Bowman *et al.*<sup>2</sup> are shown for comparison. Crosses represent  $\text{NU}(na)$ , solid circles represent  $\text{NU}(nb)$ , and the dashed curve represents the Bowman *et al.*<sup>2</sup> data. The two derived functions are essentially identical except for differences in the near-symmetric (valley) mass regions. These differences account for the differences observed in the valley region of the transformed, final mass distribution shown as circles in Figs. 3(a) and 3(b). Differences between the derived neutron-yield functions and the one of Bowman *et al.*<sup>2</sup> are discussed later.

To this point initial mass distributions  $YI(i)$  were calculated with a correction for the dependence of  $\bar{\nu}(M)$  on the total kinetic energy release  $T_{KE}$  based on the relationship,

$$\nu(M, T_{KE}) = \bar{\nu}(M) + \left\{ \bar{\nu}(M) / [\bar{\nu}(M) - \bar{\nu}(A_F - M)] \right\} \left[ \Delta_{T_{KE}} / E_n^* \right], \quad (2)$$

where  $A_F$  is the mass of the fissioning nuclide,  $E_n^*$  is the average sum of the binding energy and center-of-mass kinetic energy of the emitted neutron, taken to be 7 MeV, and  $\Delta_{T_{KE}}$  is defined as the average total kinetic energy for a given mass split,  $T_{KE}(M)$ , minus the observed total kinetic energy for the same mass split,  $T_{KE}(M)$ . Equation (2) is the  $T_{KE}(M)$ -dependence correction for neutron emission used previously at this laboratory.<sup>30,32,33</sup> However, in the course of this work it became apparent that Eq. (2) did not adequately describe the  $T_{KE}(M)$  dependence of neutron emission for all values of  $\Delta_{T_{KE}}$ , particularly large values of  $\Delta_{T_{KE}}$ . This is shown in Fig. 4 in which the number of neutrons emitted in  $^{252}\text{Cf}(sf)$  is plotted as a function of fragment mass for various values of  $\Delta_{T_{KE}}$ . The curves were deduced from the contour diagram of  $\nu$  plotted as a function of  $M$  and  $T_{KE}$  in Fig. 3(a) of Ref. 2. The solid symbols in Fig. 4 are values of  $\nu$  calculated for various values of  $M$  and  $\Delta_{T_{KE}}$  by means of Eq. (2). The open symbols in Fig. 4, showing better agreement with the deduced curves, are values calculated with a series of equations representing the  $T_{KE}(M)$  dependence of neutron emission for different values of  $\Delta_{T_{KE}}$ . For  $\Delta_{T_{KE}} \leq 0$ , Eq. (2) was

assumed to hold but with  $E_n^*$  increased from 7 to 8.5 MeV to give better agreement with the data. For  $0 < \Delta_{T_{KE}} < 20$  MeV, the correction was taken to be

$$\nu(M, T_{KE}) = \bar{\nu}(M) + (M/A_F)(\Delta_{T_{KE}}/E_n^*). \quad (3)$$

For  $20 \leq \Delta_{T_{KE}} \leq 60$  MeV,

$$\begin{aligned} \nu(M, T_{KE}) = & \bar{\nu}(M) [(60 - \Delta_{T_{KE}})/40] \\ & + (M/A_F)(\Delta_{T_{KE}}/E_n^*) \\ & + (M/A_F) [\bar{\nu}(M) + \bar{\nu}(A_F - M)] \\ & \times [1 - [(60 - \Delta_{T_{KE}})/40]]. \end{aligned} \quad (4)$$

For  $\Delta_{T_{KE}} > 60$  MeV,

$$\begin{aligned} \nu(M, T_{KE}) = & (M/A_F) [(\Delta_{T_{KE}}/E_n^*) + \bar{\nu}(M) + \bar{\nu}(A_F - M)] \\ & \times [\Delta_{T_{KE}}/60]. \end{aligned} \quad (5)$$

Equations (3)–(5) have the effect of allowing neutron emission to become more proportional to the mass of the fragment as  $\Delta_{T_{KE}}$  increases. For  $\Delta_{T_{KE}} \leq 60$  MeV some saw-toothed structure remains in the neutron-yield function. Above 60 MeV neutron emission becomes proportional to the mass of the fragment. Subsequent derivations of initial mass distributions and, hence, neutron-yield functions include the  $T_{KE}(M)$  dependence described with Eqs. (2)–(5) rather than Eq. (2) alone.

The effect of this change is shown in Fig. 3(a). The solid circles in this figure represent  $YF(na)$  obtained with Eqs. (2)–(5) used in the derivation of  $YI(na)$  and with the same  $NU(na)$  shown in Fig. 2(a) as the open circles. Only those yields in Fig. 3(a) represented by the solid circles (primarily the valley yields) change substantially from the yields represented by the open circles and are therefore the only ones plotted. Because of these changes in yield values,  $\bar{\nu}(M)$  was redetermined for  $^{252}\text{Cf}(sf)$ . The results are shown in Fig. 5:  $YF(n)$  and  $NU(n)$  are depicted by the open circles in Figs. 5(a) and 5(b), respectively. The crosses indicate  $YF(0)$  derived with the  $\bar{\nu}(M)$  of Bowman *et al.*<sup>2</sup> The  $YF(n)$  function again shows good agreement with the RC mass distribution (solid curve). The solid circles in Fig. 5(b) represent the previously described  $NU(na)$  function for those fragment masses where it deviates noticeably from the  $NU(n)$  function.

Neutron-yield functions determined for  $^{252}\text{Cf}(sf)$  by neutron counting are shown in Fig. 5(b) (crosses<sup>2</sup>) and Fig. 6 (upright triangles,<sup>4</sup> inverted triangles,<sup>6</sup> and squares<sup>8</sup>). The agreement among the various experimental determinations is quite good between masses 90–115 and 135–155. The derived neutron-yield function shown as open circles in both Fig. 5(b) and 6 exhibits general agreement

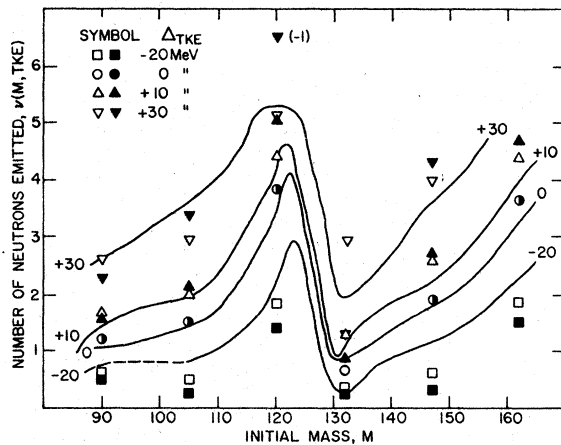


FIG. 4. Neutron emission as a function of fragment mass and  $TKE$  for  $^{252}\text{Cf}(sf)$ . The solid curves were deduced from data given in Ref. 2. The solid symbols were calculated according to Eq. (2). The open symbols were calculated according to Eqs. (2)–(5).

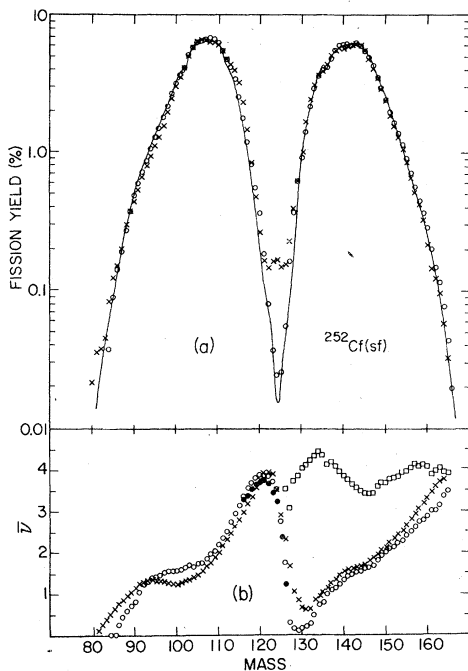


FIG. 5. (a) Final mass distributions for  $^{252}\text{Cf}(sf)$ . The solid curve represents the RC mass distribution shown in Fig. 1(a). The crosses and circles represent the transformed, starting and ending final mass distributions,  $YF(0)$  and  $YF(n)$ , respectively, derived with Eqs. (2)–(5). (b) Comparison of neutron-yield functions. Crosses represent the function determined by Bowman *et al.* (Ref. 2). Solid circles,  $NU(na)$ , were derived with Eq. (2). [See Fig. 2(a).] Open circles,  $NU(n)$ , were derived with Eqs. (2)–(5). (See text.)

with the experimental determinations. Below mass 90, the derived function is smaller in value than the other functions. At mass 95, the derived function becomes larger than the others and remains larger through mass 120. In the heavy mass region the derived function is smaller than the others from mass 127 through mass 156. Differences among the derived function and the experi-

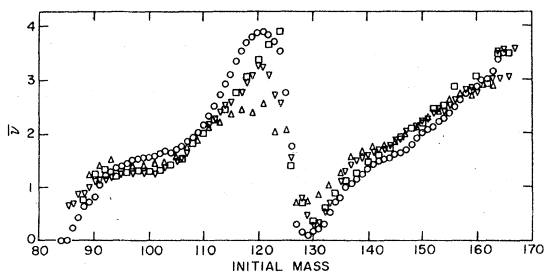


FIG. 6. Comparison of neutron-yield functions for  $^{252}\text{Cf}(sf)$ . Circles represent the derived function; upright triangles, the function determined in Ref. 4; inverted triangles, the function from Ref. 6; squares, the function from Ref. 8.

mentally determined functions are  $\sim 0.3$  neutron in the high-yield mass region. A realistic assessment of the errors in the derived neutron yield for a given mass in this region is of this magnitude. For other masses the error may be considerably larger.

#### B. Neutron-yield functions for other fissioning systems

The neutron-yield functions,  $NU(n)$ , derived for the  $^{245}\text{Cm}(n,f)$ ,  $^{254}\text{Cf}(sf)$ ,  $^{254}\text{Es}(n,f)$ -I and -II, and  $^{256}\text{Fm}(sf)$  systems are shown as circles in the lower (b) parts of Figs. 7–11, respectively. The crosses in these figures represent the  $NU(0)$  functions; the squares are the sums of the derived neutron yields for complementary fission fragments. The final mass distributions shown in the upper (a) parts of the figures represent the RC mass distribution (solid curve) and the transformed distributions,  $YF(0)$  (crosses) and  $YF(n)$  (circles). The crosses fit the RC mass distribution rather well for  $^{254}\text{Cf}(sf)$ , fairly well for  $^{245}\text{Cm}(n,f)$ , and rather poorly for  $^{254}\text{Es}(n,f)$  and  $^{256}\text{Fm}(sf)$ . The circles, as expected from the criteria for determining the "goodness" of a particular neutron-yield function, fit the RC mass

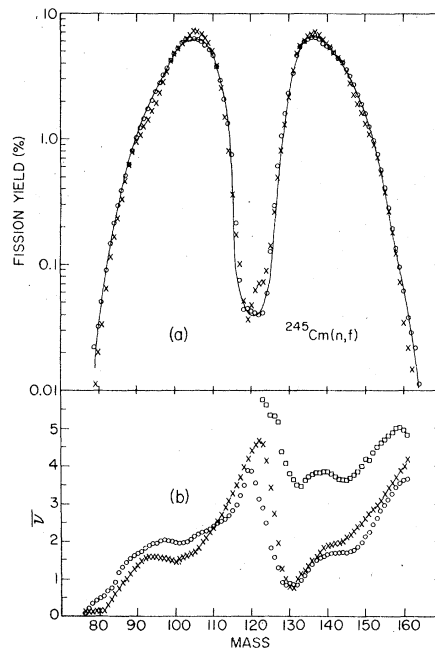


FIG. 7. (a) Final mass distributions for  $^{245}\text{Cm}(n,f)$ . The solid curve represents the RC mass distribution. Crosses and circles represent the transformed, starting and ending final mass distributions,  $YF(0)$  and  $YF(n)$ , respectively. (b) Neutron-yield functions,  $NU(0)$  (crosses) and  $NU(n)$  (circles). The squares represent the number of neutrons emitted for complementary fragment masses.

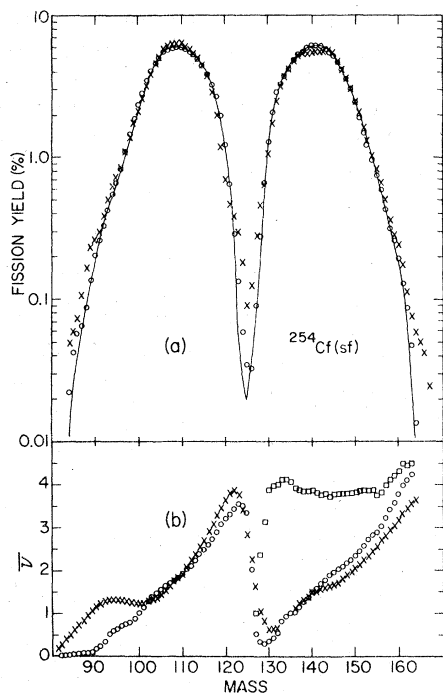


FIG. 8. (a) Final mass distributions and (b) neutron-yield functions for  $^{254}\text{Cf}(sf)$ . See Fig. 7 for the description of symbols.

distributions quite well.

In Figs. 9 and 10 one observes the effect of different final mass distributions on the derivation of  $\bar{\nu}(M)$  for  $^{254}\text{Es}(n,f)$ . In Fig. 10(b) both neutron-yield functions corresponding to RC mass distribu-

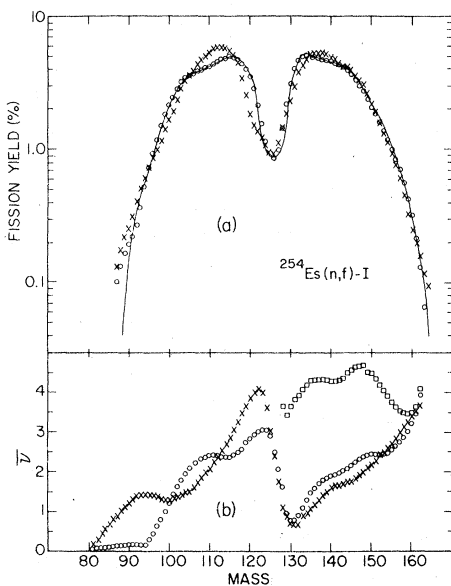


FIG. 9. (a) Final mass distributions and (b) neutron-yield functions for  $^{254}\text{Es}(n,f)$ -I. See Fig. 7 for the description of symbols.

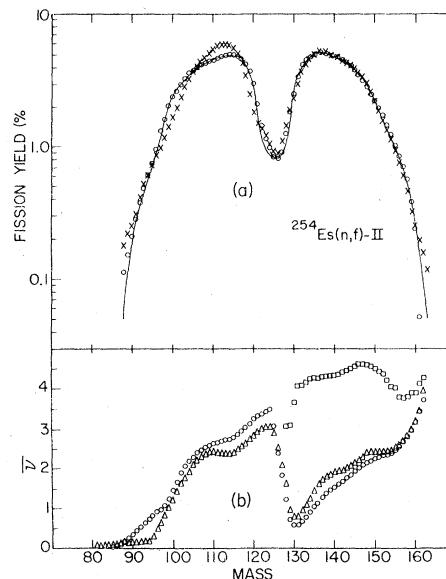


FIG. 10. (a) Final mass distributions and (b) neutron-yield functions for  $^{254}\text{Es}(n,f)$ -II. See Fig. 7 for the description of symbols. The triangles in (b) represent the neutron-yield function derived for  $^{254}\text{Es}(n,f)$ -I [Fig. 9(b)] and are shown for comparison.

tions I and II are plotted as triangles and circles, respectively. Differences between the two functions are sizable, as much as 0.5 neutron at masses 94, 124, and 136. Since  $\bar{\nu}(M)$  depends on both initial and final mass distributions, it is estimated that  $\bar{\nu}(M)$  for  $^{254}\text{Es}(n,f)$  and  $^{256}\text{Fm}(sf)$  have an uncertainty of 0.7 neutron in the worst case, i.e., in far asymmetric and near-symmetric mass regions. The uncertainties for the other fissioning

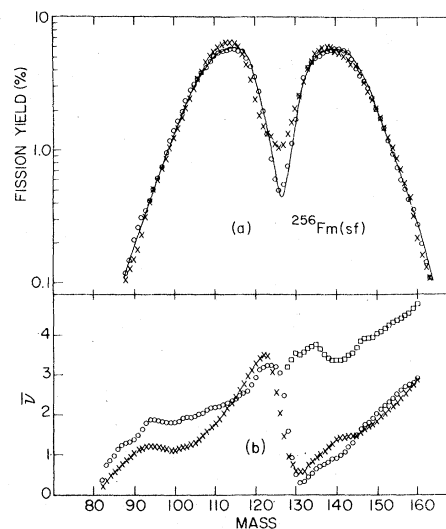


FIG. 11. (a) Final mass distributions and (b) neutron-yield functions for  $^{256}\text{Fm}(sf)$ . See Fig. 7 for the description of symbols.

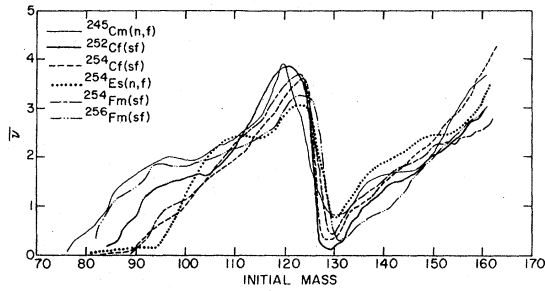


FIG. 12. Derived neutron-yield functions shown for comparison. The function for  $^{254}\text{Fm}(sf)$  is from Ref. 46.

systems are estimated to be less than this, varying downward to 0.3 neutron for  $^{252}\text{Cf}(sf)$  in the high-yield mass regions.

The derived neutron-yield functions for  $^{252}\text{Cf}(sf)$ ,  $^{245}\text{Cm}(n,f)$ ,  $^{254}\text{Cf}(sf)$ ,  $^{254}\text{Es}(n,f)$ -I,  $^{256}\text{Fm}(sf)$ , and  $^{254}\text{Fm}(sf)$ <sup>46</sup> are shown for comparison in Fig. 12. The saw-toothed character is obvious in all six functions. Maximum neutron emission occurs for masses 119–124; whereas minimum neutron emission occurs for masses 129–132. Masses for which maximum and minimum neutron emission occur are given for each fissioning system in Table III. The minima in  $\bar{\nu}(M)$  for  $^{245}\text{Cm}(n,f)$  and  $^{254}\text{Es}(n,f)$  are not as deep as the minima for the (sf) systems. It is tempting to attribute this to the increased nuclear excitation in the (n,f) systems compared with the (sf) systems. However, this may be too simplified an approach. Rather, a direct comparison should be made of the neutron-yield functions obtained for  $^{245}\text{Cm}(n,f)$  and  $^{246}\text{Cm}(sf)$  whenever sufficient data become available for the latter system. It should also be noted that  $\bar{\nu}_T$  for  $^{254}\text{Es}(n,f)$  is based on the systematics<sup>27</sup> of neutron emission rather than on an experimental number. The value of 4.26 agrees well, however, with the values (Table III) determined indirectly from dif-

ferences in the first moments of the light and heavy mass groups of initial and final mass distributions.

Other than the general saw-tooth shapes of the  $\bar{\nu}(M)$  curves, it would be difficult to claim a “universality” among them. There is a general increase in neutron emission with fragment mass in the heavy mass region. The approximate slope of a linear envelope about the curves in this region is about 0.09 neutron per mass unit. The height of such an envelope is about one neutron. In the light mass region there is less uniformity among the curves.

The saw-tooth feature of the  $\bar{\nu}(M)$  curves and the similarity or lack of similarity among them can be interpreted qualitatively by a consideration of shells in deformed fragment nuclei.<sup>47</sup> To a first approximation the number of neutrons emitted by a fission fragment is proportional to the excitation energy of the fragment and this in turn depends largely on the deformation of the fragment at scission. Thus a fragment that is largely deformed will emit a larger number of neutrons than one that is only slightly deformed. The scission-point model of fission<sup>47</sup> indicates that the total deformation of various fragment pairs for a given fissioning system is nearly constant. From the contour plot of the potential energy surface as a function of the two fragment deformations in Fig. 4 of Ref. 47, it is apparent that the fission fragments can deform more readily in the direction of constant total deformation than in an opposite direction in which both fragments become either more spherical or more deformed. Because of the near constancy of the total deformation one expects that fragments which emit the fewest and the most neutrons to be complementary. From Table III one observes that with the exception of  $^{245}\text{Cm}(n,f)$ , the masses for which maximum and minimum neutron emission occur are complement-

TABLE III. Characteristics of neutron emission for various fissioning systems.

Fissioning system	Symmetric mass, $A_F/2$	Max. $\bar{\nu}$ (Mass)	Min. $\bar{\nu}$ (Mass)	Sum <sup>a</sup> (Mass)	$\bar{\nu}_L$ <sup>b</sup>	$\bar{\nu}_H$ <sup>b</sup>	$\bar{\nu}_T$ <sup>c</sup>
$^{245}\text{Cm}(n,f)$	123	119	132	251	2.3	1.6	3.9
$^{252}\text{Cf}(sf)$	126	121	129	250	2.2	1.5	3.7
$^{254}\text{Cf}(sf)$	127	123, 124	129	252, 253	2.1	1.8	3.9
$^{254}\text{Es}(n,f)$ -I	127.5	123	130	253	2.3	2.0	4.3
$^{254}\text{Es}(n,f)$ -II	127.5	124	131	255	2.6	1.8	4.4
$^{254}\text{Fm}(sf)$ <sup>d</sup>	127	123	129, 130	252, 253	2.2	1.7	3.9
$^{256}\text{Fm}(sf)$	128	124	131	255	2.5	1.3	3.8

<sup>a</sup>Sum of masses for which maximum and minimum neutron emission occurs.

<sup>b</sup>Average number of neutrons emitted from the light (L) or heavy (H) fragments deduced from differences in the first moments of the mass groups in initial and final mass distributions.

<sup>c</sup> $\bar{\nu}_T = \bar{\nu}_L + \bar{\nu}_H$ .

<sup>d</sup>Data from Ref. 46.

ary within  $\pm 2$  mass units. For  $^{245}\text{Cm}(n,f)$  the calculated minimum neutron emission is at mass 132 and is 0.83 neutron per fission. The calculated value at mass 129 is 0.84 neutron per fission. In view of the uncertainties discussed previously, it would be difficult to state categorically that minimum neutron emission occurs at mass 132 rather than 129. Minimum neutron emission at mass 129, of course, is more nearly the complement of mass 119 for the  $^{245}\text{Cm}(s,f)$  system and more in keeping with the other fissioning systems as far as complementarity is concerned. However, deviations from complementarity may be caused by a number of factors. Two of the most obvious are that (1) the total deformation for a given fissioning system is not exactly constant for all pairs of fission fragments, and (2) the data used in the derivation of a given  $\bar{\nu}(M)$  are not sufficiently accurate to discern the true maximum or minimum. We are not prepared at present to defend one factor to the exclusion of the other.

The region of minimum neutron emission is associated with masses in which both strong proton ( $Z=50$ ) and neutron ( $N=82$ ) shells occur for spherical nuclei.<sup>47</sup> Minimum neutron emission does not necessarily occur at mass 132 because liquid drop forces tend to form fragments with the same mass-to-proton ratio to within 0.5  $Z$  unit as the fissioning nuclide. For  $Z=50$ , liquid drop forces would tend to give fragments with  $N=78-81$  for the systems given in Table II; similarly for  $N=82$ , fragments with  $Z=51-52$  would be preferred.

In the mass region of the fission fragments the influence of the neutron shells predominate over that of the proton shells and, to a first approximation, the neutron shells associated with the heavy fragments are stronger than those associated with the light fragment, particularly those shells with 82 and 88 neutrons located at  $\beta$  deformations of approximately 0.1 and 0.65, respectively.<sup>47</sup> Therefore, since neutron emission for the systems discussed in the present paper depends primarily on fragment deformation, one might expect neutron emission by the heavy fragment to be similar for the various systems. Differences would occur because of variations in (1) the mass-to-proton ratio, (2) the intrinsic excitation energy of the system at the moment the mass distribution is determined, and most importantly (3) the preferred deformation of the various complementary fragments. For example, if a complementary (light) fragment has a strong shell at a small deformation, the heavy fragment, because of the nearly constant total deformation of the two fragments, tends to be more deformed and to emit more neutrons. Conversely, the heavy fragment

may emit fewer neutrons if the light fragment has a strong shell at a large deformation. Figure 12 indicates a similarity in the shapes of the neutron-yield curves for the heavy fragment in the various fissioning systems. The lack of uniformity in neutron emission by the light fragment (Fig. 12) is then largely the result of the light fragment varying more in mass and neutron number from system to system than the heavy fragment. Because of this greater variation different neutron shells come into play in the light fragment for each fissioning system and cause different neutron emission patterns.

The average number of neutrons emitted by light  $\bar{\nu}_L$  or heavy  $\bar{\nu}_H$  fragments for a particular fissioning system can be calculated by subtracting the average light or heavy mass in the final mass distribution from the corresponding average mass in the initial mass distribution. Values of  $\bar{\nu}_L$  and  $\bar{\nu}_H$  determined in this manner are given in Table III. These values indicate that, except for  $^{254}\text{Cf}(sf)$  and  $^{254}\text{Es}(n,f)-I$ , significantly more neutrons are emitted from light fragments than from heavy fragments. The experimental results of Bowman *et al.*<sup>2</sup> indicate a  $\bar{\nu}_L/\bar{\nu}_H$  ratio of only  $1.17 \pm 0.03$  for  $^{252}\text{Cf}(sf)$  compared to the 1.47 value deduced from the values given in Table II. These differences are readily accounted for by the differences shown in Figs. 5(b) and 6 between the derived neutron-yield function and the experimentally measured neutron-yield functions in the light and heavy mass regions.

The values of  $\bar{\nu}_T = \bar{\nu}_L + \bar{\nu}_H$  given in Table III agree well with the values of  $\bar{\nu}_T$  listed in Table I which were used in the calculation of  $\bar{\nu}(M)$ .

#### C. Effect of $\bar{\nu}(M)$ on the derivation of various mass and energy distributions

In a previous paper<sup>30</sup> initial mass distributions,  $T_{KE}$  as a function of fragment mass [ $T_{KE}(M)$ ], and the dispersion in  $T_{KE}(M)$  as a function of fragment mass ( $\sigma_{T_{KE}(M)}$ ) were presented for a number of fissioning systems. The initial masses were deduced from KE measurements with the assumptions (1) that the neutron-yield function for fissioning systems with  $Z \geq 96$  had the same shape as the  $^{252}\text{Cf}(sf)$  neutron-yield function determined by Bowman *et al.*<sup>2</sup> and (2) that the  $T_{KE}$  dependence for neutron emission was described by Eq. (2). Examples of these distributions are shown as crosses in Figs. 13-17. The same types of distributions but deduced with the neutron-yield functions derived in the present paper and with the assumption that the  $T_{KE}$  dependence for neutron emission is described by Eqs. (2)-(5) are shown as circles in Figs. 13-17. In Fig. 16 the solid

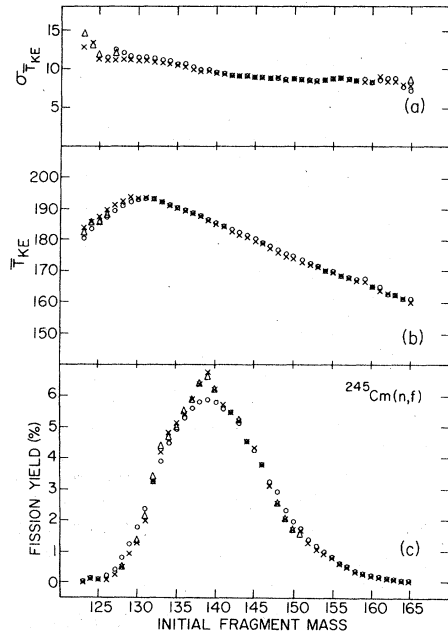


FIG. 13. (a) Root-mean-square of the total kinetic energy distribution as a function of fragment mass, (b) average total kinetic energy as a function of fragment mass, and (c) the initial mass distribution for  $^{245}\text{Cm}(n,f)$ . Open circles represent data calculated with the derived neutron-yield function and Eqs. (2)–(5). Crosses represent data calculated with an assumed  $^{252}\text{Cf}(sf)$ -shaped neutron-yield function and Eq. (2). Open triangles represent data calculated with an assumed  $^{252}\text{Cf}(sf)$ -shaped neutron-yield function and Eqs. (2)–(5). The triangles are shown in this figure and in Fig. 17 and are plotted only where they differ noticeably from the crosses.

circles represent values calculated with the  $^{254}\text{Es}(n,f)$ -II neutron-yield function where they differ noticeably from the values calculated with the  $^{254}\text{Es}(n,f)$ -I function. There is a consistent pattern between the  $\bar{T}_{\text{KE}}(M)$  distributions calculated with the previous (crosses) and present (circles) method as well as between the  $\sigma_{T_{\text{KE}}(M)}$  distributions calculated with the two methods. In the region of the most probable mass there is, in general, little difference between the results obtained with the two methods. However, as one approaches symmetry, the circles indicate smaller values than the crosses for  $\bar{T}_{\text{KE}}(M)$  and larger values for  $\sigma_{T_{\text{KE}}(M)}$ . Since the symmetric yields represent only a small percentage of the total fission yield, the old assumptions can be used to calculate  $\bar{T}_{\text{KE}}(M)$  and  $\sigma_{T_{\text{KE}}(M)}$  rather well for fissioning systems from  $^{246}\text{Cm}$  to  $^{256}\text{Fm}$ .

The initial mass distributions show greater differences when calculated with the previous and present method than do  $\bar{T}_{\text{KE}}(M)$  or  $\sigma_{T_{\text{KE}}(M)}$ . In  $^{245}\text{Cm}(n,f)$  [Fig. 13(c)] the circles indicate considerably less yield at masses 136–139 than do

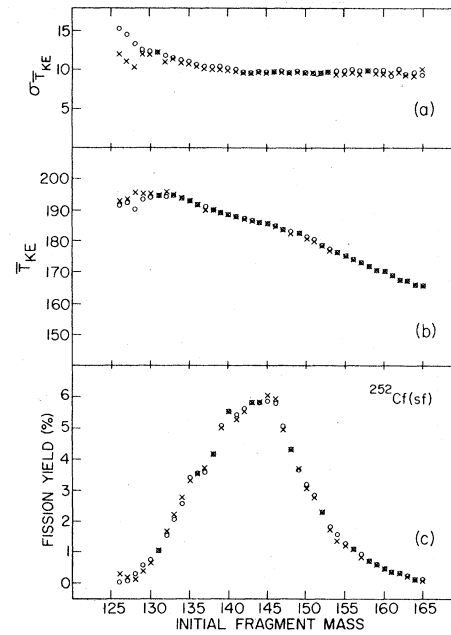


FIG. 14. (a) Root-mean-square of the total kinetic energy distribution as a function of fragment mass, (b) the average total kinetic energy as a function of fragment mass, and (c) the initial mass distribution for  $^{252}\text{Cf}(sf)$ . See Fig. 13 for the description of symbols.

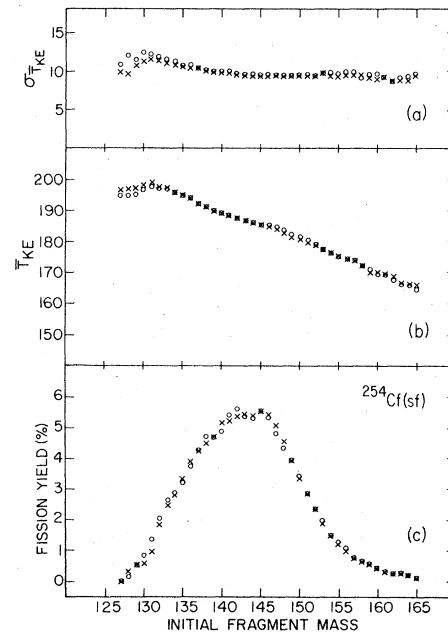


FIG. 15. (a) Root-mean-square of the total kinetic energy distribution as a function of fragment mass, (b) the average total kinetic energy as a function of fragment mass, and (c) the initial mass distribution for  $^{254}\text{Cf}(sf)$ . See Fig. 13 for the description of symbols.

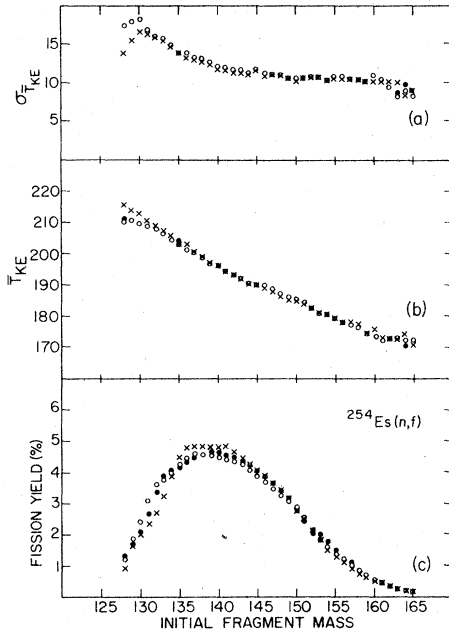


FIG. 16. (a) Root-mean-square of the total kinetic energy distribution as a function of fragment mass, (b) the average total kinetic energy as a function of fragment mass, and (c) the initial mass distribution for  $^{254}\text{Es}(n,f)$ . The open circles are for  $^{254}\text{Es}(n,f)$ -I. The closed circles are for  $^{254}\text{Es}(n,f)$ -II and are shown only where they differ noticeably from the open circles. A description of the values represented by circles and crosses is given with Fig. 13.

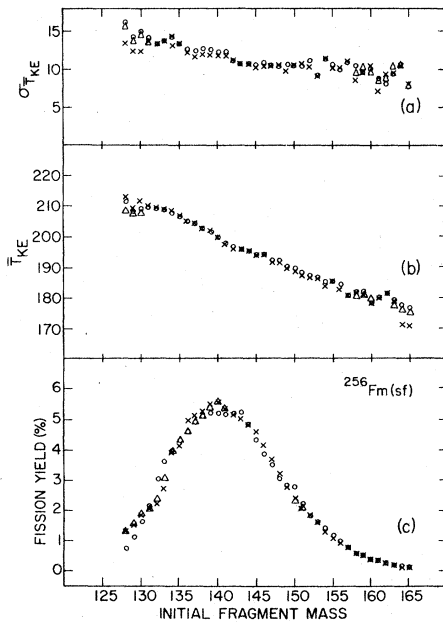


FIG. 17. (a) Root-mean-square of the total kinetic energy distribution as a function of fragment mass, (b) the average total kinetic energy as a function of fragment mass, and (c) the initial mass distribution for  $^{256}\text{Fm}(sf)$ . See Fig. 13 for the description of symbols.

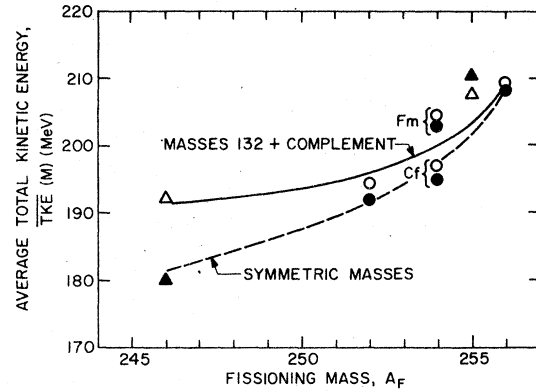


FIG. 18. The variation of  $\bar{T}_{KE}$  for fragment mass 132 plus its complement (open symbols) and symmetric fission fragment masses (closed symbols) as a function of fissioning mass. Circles are for spontaneous fissioning systems. Triangles are for thermal-neutron-induced fissioning system. The solid and dashed curves indicate the general trend for the open and solid symbols, respectively.

the crosses. For  $^{252}\text{Cf}(sf)$  and  $^{254}\text{Cf}(sf)$  [Figs. 14(c) and 15(c), respectively] there is not much difference between the crosses and circles. For  $^{254}\text{Es}(n,f)$  [Fig. 16(c)] there are significant differences between the previous and present distributions for both the I and II distributions. For  $^{256}\text{Fm}(sf)$  [Fig. 17(c)] there are noticeable differences. Thus the old assumptions may or may not be too reliable in calculating the initial mass distribution, depending on the fissioning system and the accuracy which one desires.

It should be remembered that the values represented by crosses and circles in Figs. 13–17 are the result of two changes: (1) different neutron-yield functions and (2) different equations representing the  $T_{KE}$  dependence of neutron emission. The effect of changing just the  $T_{KE}$  dependence of neutron emission is shown in Figs. 13 and 17 for  $^{245}\text{Cm}(n,f)$  and  $^{256}\text{Fm}(sf)$ . In these figures, the triangles represent values of  $\sigma_{T_{KE}(M)}$ ,  $\bar{T}_{KE}(M)$ , and initial mass-yield that were calculated with the assumption that the neutron-yield function have the same shape as the one determined for  $^{252}\text{Cf}(sf)$  by Bowman *et al.*<sup>2</sup> (previous assumption) but that the  $T_{KE}$  dependence for neutron emission is described by Eqs. (2)–(5) (present assumption). One notes that near symmetry these values are smaller for  $\bar{T}_{KE}(M)$  and greater for  $\sigma_{T_{KE}(M)}$  than are the corresponding values represented by the crosses. The initial mass yields, however, are very similar.

Figure 18 is a plot of the  $\bar{T}_{KE}(M)$  values for  $M=132$  plus its complementary fission fragment mass (open symbols) and for symmetric fission fragment masses (closed symbols) for the five fissioning systems. The general trend of  $\bar{T}_{KE}(M)$

for the two types of mass split as indicated by the solid and dashed curves is in keeping with that predicted by the scission-point model of fission (see Fig. 18 of Ref. 47).

This work was performed under the auspices of the U. S. Department of Energy. It is with great gratitude that I acknowledge my co-authors in

Ref. 30 for making available to me the kinetic energy measurements described in that paper. In particular I wish to thank Dr. L. Glendenin and Dr. J. Unik for their comments on the paper and to the latter for the use of computer programs developed by him. The critical comments of Dr. B. Wilkins and discussion with him about the scission-point model of fission were very helpful.

- <sup>1</sup>S. L. Whetstone, Phys. Rev. **114**, 481 (1959).
- <sup>2</sup>H. R. Bowman, J. C. D. Milton, S. G. Thompson, and W. J. Swiatecki, Phys. Rev. **129**, 3122 (1963).
- <sup>3</sup>E. Nardi and Z. Fraenkel, Phys. Rev. Lett. **20**, 1248 (1968).
- <sup>4</sup>A. Gavron and Z. Fraenkel, Phys. Rev. Lett. **27**, 114 (1971); Phys. Rev. C **9**, 632 (1974).
- <sup>5</sup>C. Signarbieux, J. Poitou, M. Ribrag, and J. Matussek, Phys. Lett. **39B**, 503 (1972).
- <sup>6</sup>C. Signarbieux, H. Nifenecker, J. Poitou, and M. Ribrag, J. Phys. (Paris) Suppl. **8-9**, C 5 (1972).
- <sup>7</sup>C. Signarbieux, R. Babinet, H. Nifenecker, and J. Poitou, in *Proceedings of the Third International Atomic Energy Agency Symposium on the Physics and Chemistry of Fission, Rochester, 1973* (IAEA, Vienna, 1974), Vol. 2, p. 179.
- <sup>8</sup>R. L. Walsh and J. W. Boldeman, Nucl. Phys. **A276**, 189 (1977).
- <sup>9</sup>V. F. Apalin, Yu. N. Gritsyuk, I. E. Kutikov, V. I. Lebedev, and L. A. Mikaelyan, in *Proceedings of the First International Atomic Energy Agency Symposium on Physics and Chemistry of Fission, Salzburg, 1965* (IAEA, Vienna, 1965), Vol. 1, p. 587; Yad. Fiz. **1**, 639 (1965); Sov. J. Nucl. Phys. **1**, 457 (1965); Nucl. Phys. **71**, 553 (1965).
- <sup>10</sup>J. C. D. Milton and J. S. Fraser, in *Proceedings of the First International Atomic Energy Agency Symposium on Physics and Chemistry of Fission, Salzburg, 1965* (IAEA, Vienna, 1965), Vol. 2, p. 39.
- <sup>11</sup>V. F. Apalin, Yu. N. Gritsyuk, I. E. Kutikov, V. I. Lebedev and L. A. Mikaelyan, Zh. Eksp. Theor. Fiz. **46**, 1197 (1964) [Sov. Phys. JETP **46**, 810 (1964)]; Nucl. Phys. **55**, 249 (1964).
- <sup>12</sup>T. Cornall, E. E. Maslin, and A. L. Rodgers, see Ref. 10, Vol. 2, p. 67.
- <sup>13</sup>J. S. Fraser and J. C. D. Milton, Annu. Rev. Nucl. Science **16**, 379 (1966).
- <sup>14</sup>E. E. Maslin, A. L. Rodgers, and W. G. F. Core, Phys. Rev. **164**, 1520 (1967).
- <sup>15</sup>J. W. Boldeman, A. R. de L. Musgrove, and R. L. Walsh, Aust. J. Phys. **24**, 821 (1971).
- <sup>16</sup>W. E. Stein, see Ref. 10, Vol. 1, p. 491.
- <sup>17</sup>H. W. Schmitt, W. E. Kiker, and C. W. Williams, Phys. Rev. **137**, B837 (1965).
- <sup>18</sup>H. W. Schmitt, R. W. Lide, and F. Pleasonton, Nucl. Instrum. Methods **63**, 237 (1968).
- <sup>19</sup>M. Derengowski and E. Malkonian, Phys. Rev. C **2**, 1554 (1970).
- <sup>20</sup>H. Hipp, H. Henschel, and G. Goennenwein, see Ref. 7, Vol. 2, p. 483.
- <sup>21</sup>H. Yamamoto, Y. Mori, Y. Wakuta, and M. Senoda, Nucl. Instrum. Methods **134**, 119 (1976).
- <sup>22</sup>J. Terrell, Phys. Rev. **127**, 880 (1962); see Ref. 10, Vol. 2, p. 3.
- <sup>23</sup>H. Farrar and R. H. Tomlinson, Can. J. Phys. **40**, 943 (1962).
- <sup>24</sup>J. Blachot, P. Cavallini, A. Ferrieu, and R. Louis, J. Radioanal. Chem. **26**, 107 (1975).
- <sup>25</sup>A. C. Wahl, A. E. Norris, R. A. Rouse, and J. C. Williams, in *Proceedings of the Second International Atomic Energy Symposium on Physics and Chemistry of Fission, Vienna, 1969* (IAEA, Vienna, 1969), p. 813.
- <sup>26</sup>G. C. Hanna, C. H. Westcott, H. D. Lemmel, B. P. Leonard, Jr., J. S. Story, and P. M. Attree, At. Energ. Rev. **7**, #4, 3 (1969).
- <sup>27</sup>A. H. Jaffey and J. L. Lerner, Nucl. Phys. **A145**, 1 (1970).
- <sup>28</sup>F. Manero and V. A. Konshin, At. Energ. Rev. **10**, #4, 637 (1972).
- <sup>29</sup>M. Dakovskii, Yu. A. Lazarev, and Yu. Ts. Oganessian, Yad. Fiz. **16**, 1167 (1972); Sov. J. Nucl. Phys. **16**, 641 (1973).
- <sup>30</sup>J. P. Unik, J. E. Gindler, L. E. Glendenin, K. F. Flynn, A. Gorski, and R. K. Sjoblom, see Ref. 7, Vol. 2, p. 19.
- <sup>31</sup>H. W. Schmitt, J. H. Neiler, and F. J. Walters, Phys. Rev. **141**, 1146 (1966).
- <sup>32</sup>L. E. Glendenin, H. C. Griffin, W. Reisdorf, and J. P. Unik, see Ref. 25, p. 781.
- <sup>33</sup>W. Reisdorf, J. P. Unik, H. C. Griffin, and L. E. Glendenin, Nucl. Phys. **A177**, 337 (1971).
- <sup>34</sup>K. F. Flynn, J. E. Gindler, and L. E. Glendenin, J. Inorg. Nucl. Chem. **37**, 881 (1975).
- <sup>35</sup>W. E. Nervik, Phys. Rev. **119**, 1685 (1960).
- <sup>36</sup>R. M. Harbour, M. Eichor, and D. E. Troutner, Radiochim. Acta **15**, 146 (1971).
- <sup>37</sup>N. V. Skovorodkin, G. E. Kozhkomoev, K. A. Petrzhak, A. V. Sorokina, B. M. Alexandrov, and A. S. Krivokhatski, At. Energ. **34**, 365 (1973) [Sov. At. Energ. **34**, 449 (1973)].
- <sup>38</sup>B. Srinivasan, E. C. Alexander, O. K. Manuel, and D. E. Troutner, Phys. Rev. **179**, 1166 (1969).
- <sup>39</sup>H. R. von Gunten, K. F. Flynn, and L. E. Glendenin, Phys. Rev. **161**, 1192 (1967).
- <sup>40</sup>R. M. Harbour and K. W. MacMurdo, J. Inorg. Nucl. Chem. **34**, 2109 (1972).
- <sup>41</sup>W. H. Walker, in *Proceedings of the International Atomic Energy Agency Panel on Fission Product Data, Bologna, 1973* (IAEA, Vienna, 1974), Vol. 1, p. 285.
- <sup>42</sup>K. Flynn, J. Gindler, L. Glendenin, A. Gorski, R. Sjoblom, and J. P. Unik, in proceedings of the 167th American Chemical Society National Meeting, Los Angeles, 1974 (unpublished).

- <sup>43</sup>K. Wolfsberg and G. P. Ford, in proceedings of the 167th American Chemical Society National Meeting, Los Angeles, 1974 (unpublished).
- <sup>44</sup>K. F. Flynn, J. E. Gindler, L. E. Glendenin, and R. K. Sjoblom, *J. Nucl. Inorg. Chem.* 38, 661 (1976).
- <sup>45</sup>K. F. Flynn, E. P. Horwitz, C. A. A. Bloomquist, R. F. Barnes, R. K. Sjoblom, P. R. Fields, and L. E. Glendenin, *Phys. Rev. C* 5, 1725 (1972).
- <sup>46</sup>J. E. Gindler, K. F. Flynn, L. E. Glendenin, and R. K. Sjoblom, *Phys. Rev. C* 16, 1483 (1977).
- <sup>47</sup>B. D. Wilkins, E. P. Steinberg, and R. R. Chasman, *Phys. Rev. C* 14, 1832 (1976).
- <sup>48</sup>D. C. Hoffman and M. M. Hoffman, *Annu. Rev. Nucl. Sci.* 24, 151 (1974).